Supplement of Atmos. Chem. Phys., 24, 9177–9195, 2024
https://doi.org/10.5194/acp-24-9177-2024-supplement

Atmospheric Chemistry and Physics
Open Access
EGU

Supplement of

Investigation of the impact of satellite vertical sensitivity on long-term retrieved lower-tropospheric ozone trends

Richard J. Pope et al.

Correspondence to: Richard J. Pope (r.j.pope@leeds.ac.uk)

S1: Ozonesondes and Averaging Kernels

We have used ozonesonde data between 2008 and 2017 from the World Ozone and Ultraviolet Radiation Data Centre (WOUDC, https://woudc.org/), the Southern Hemisphere ADditional Ozonesondes (SHADOZ) project (https://tropo.gsfc.nasa.gov/shadoz/) and from the National Oceanic and Atmospheric Administration (NOAA, https://gml.noaa.gov/ozwv/ozsondes/). The ozonesonde locations are shown in **Figure S1.** Here, a month-latitude long-term set of bias corrections offsets (BCOs) has been generated in 30° latitude bins for 12-months (i.e. a climatological of monthly averages) over the record for each instrument (i.e. subtraction term in units of Dobson units, DU). As satellite records can have systematic biases in column ozone (e.g. Gaudel et al., 2018), we use these BCOs in an attempt to harmonise the records in absolute value terms. Thus, as the BCOs are generated from a long-term average, they should improve absolute column values, but not interfere with the long-term change in the record. This was done for lower tropospheric column ozone ($LTCO_3$), as discussed in the main manuscript.

To derive the BCOs, each ozonesonde profile was spatiotemporally co-located with the nearest satellite retrieval within 500 km and 6 hours to allow for robust comparisons and reduce sampling errors. Here, O_3 measurements were rejected if the O_3 or pressure values were unphysical (i.e. < 0.0), if the O_3 partial pressure > 2000.0 or the O_3 value was set to 99.9, and whole ozonesonde profiles were rejected if least 50% of the measurements did not meet these criteria. These criteria are similar to those applied by Keppins et al., (2018) and Hubert et al., (2016). To allow for direct like-for-like comparisons between the two quantities, accounting for the vertical sensitivity of the satellite, the instrument averaging kernels (AKs) are applied to the ozonesonde profiles. Firstly, the co-located ozonesonde profile (in volume mixing ratio) is interpolated onto the satellite pressure grid in $\log(pressure)$. The sonde sub-columns are then derived using the hydrostatic balance approximation:

$$mass\ density = mmr \times \rho \times dz = mmr \times \frac{-dp}{g} \qquad (1)$$

where *mass density* is mass (kg) of O_3 per m^2 between two pressure levels, *mmr* is the O_3 mass mixing ratio from the sonde, ρ is the density (kg/m^3), *dz* is the distance (m) between pressure levels, *dp* is the pressure difference (Pa) between levels and *g* is the acceleration due to gravity (-9.81 m/s^2). The application of the AKs for the Ozone Monitoring Instrument (OMI**)** and the Infrared Atmospheric Sounding Interferometer products (IASI) are:

$$\boldsymbol{sonde_{AK} = AK(sonde_{int} - apr) + apr} \qquad (2)$$

where $\boldsymbol{sonde_{AK}}$ is the modified ozonesonde sub-column profile (Dobson units, DU), ***AK*** is the averaging kernel matrix, $\boldsymbol{sonde_{int}}$ is the sonde sub-column profile (DU) on the satellite pressure grid and ***apr*** is the apriori (DU). The application of the satellite AKs to the UKESM model profiles is the same. The only differences are that for each satellite retrieval, the closest UKESM grid box is used and is within 3-hours.

For the RAL OMI products, the data is already represented as $LTCO_3$ in the lowest layer. For the IASI products, given its greater vertical resolutions, the sub-columns between levels were totalled up to the 450 hPa layer for the $LTCO_3$. The satellite and ozonesonde, with AKs applied, $LTCO_3$ quantities were then binned into the respective latitude and monthly bins and the median biases (satellite-ozonesonde) or offsets were determined. Therefore, whenever the satellite datasets listed in **Table 1** of the main manuscript are used (e.g. for trends or comparison with UKESM), the BCOs are

subtracted from the satellite data for the relevant latitude and monthly bins. The OMI, IASI-FORLI and IASI-SOFRID $LTCO_3$ BCOs are shown in **Figure S2**, **Figure S3** and **Figure S4**, respectively.

S2: HTAP Mask

The Hemispheric Transport of Air Pollution (HTAP) Task Force, in 2012, launched a co-ordinated multi-model and analysis programme (HTAP Phase 2) to help inform the Convention on Long-range Transboundary Air Pollution (LRTAP), national governments and multi-lateral cooperative efforts on appropriate actions to decrease air pollutant and its associated impacts (European Commission, 2016). Within HTAP Phase 2, a useful land mask was developed (**Figure S5**) to focus analysis on sub-global regions. Each region is assigned a code, so regions of e.g. O_3 data can be extracted from datasets, on the same spatial resolution of the HTAP mask, and averaged together to derive regional quantity time-series for analysis. This is a more robust approach than using a square/rectangular longitudinal-latitudinal box to approximate an area of interest. The subsequent satellite-UKESM trend and seasonal cycle analyses in **Section 3** of the main manuscript uses this HTAP mask to derive regional information.

S3: Satellite Degrees of Freedom of Signal

The degrees of freedom of signal (DOFS) represent the number of independent pieces of information from a satellite retrieval over a specified altitude range (e.g. total column, tropospheric column or lower tropospheric column (surface to 450 hPa) in this study). Here, we have used the satellite AKs to derive the $LTCO_3$ DOFS (i.e. trace of the AK matrix over the relevant satellite levels) and investigate how they have changed with time (**Figure S6**). For North America and Europe, the OMI and IASI-FORLI DOFS are approximately 0.5-0.7 and 0.3-0.5, respectively. However, for East Asia, their DOFS decrease to approximately 0.4-0.5 and 0.2-0.4, respectively. IASI-SOFRID typically has slightly lower DOFS, ranging between 0.2-0.4 across all three regions.

The long-term (2008-2017) trends in DOFS for all the products are relatively small ranging between -0.66 and 0.57 %/year. Only OMI shows substantial trends (i.e. p-value < 0.05) for North America and Europe. Overall, the $LTCO_3$ DOFS trends are small suggesting limited changes in the $LTCO_3$ information content of all the products and thus, unlikely to be contributing to the long-term $LTCO_3$ trends for the satellite records studies here.

S4: UKESM Evaluation

For comparison with the ozonesondes (**Figure S7**), the model was co-located in time (within 6 hours) and space (nearest model grid box) with each of the ozonesondes. The analysis has been split up into three latitude ranges (90-30°S, 30°S-30°N & 30-90°N) and four seasons (December-January-February (DJF), March-April-May (MAM), June-July-August (JJA) and September-October-November (SON)). In the northern hemisphere (30-90°N), correlations range between 0.67 and 0.76 across the seasons with a relatively small percentage mean bias (MB%) of -12.94% to 4.39%. In the tropics (30°S-30°N), correlations range from 0.52 to 0.70 across the seasons with larger MB% values of 15.38% to 21.98%. The southern hemisphere (90-30°S) exhibits the strongest correlations between the model and observations, ranging between 0.72 and 0.90. The model underestimates $LTCO_3$, with MB% values of -22.28% to -8.79%. Overall, UKESM reproduces reasonably well the latitudinal-seasonal variations recorded in the ozonesondes for $LTCO_3$.

UKESM (with the corresponding AKs applied) was compared with OMI, IASI-FORLI and IASI-SOFIRD $LTCO_3$ for DJF and JJA between 2008 and 2017. Note, the ozonesonde BCOs have been applied to all the satellite products. In comparison to OMI (**Figure S8**), UKESM typically simulates the $LTCO_3$ spatial

distribution and seasonality. In DJF, UKESM has both regional negative (-3.0 DU to 0.0 DU) and positive (0-3.0 DU) biases, while in JJA there are widespread biases of 0.0-4.0 DU over the tropics and sub-tropics. However, in general, the absolute UKESM-OMI biases sit within the satellite uncertainty ranges. When compared to IASI-FORLI (**Figure S9**), UKESM simulates similar spatial distributions and seasonality, but largely underestimates the retrieved $LTCO_3$ by 3.0-5.0 DU. These biases tend to be classed as "substantial" biases as the absolute bias is often larger than the retrieved $LTCO_3$ uncertainty range. These low biases are most prominent over the high-latitudes (-5.0 to -3.0 DU). Against IASI- SOFRID (**Figure S10**), the comparisons become more complex due to the $LTCO_3$ latitudinal banding caused by the dynamic apriori used in the retrieval scheme. This is potentially suggestive that IASI-SOFRID has less vertical sensitivity in the surface-450 hPa range in comparison to the other products. In general, UKESM overestimates $LTCO_3$ by 2.0 to 4.0 DU, but some regions are more substantial (e.g. northern sub-tropics in DJF, >5.0 DU, and in the Middle East/southern Africa in JJA, > 5.0 DU). Overall, UKESM robustly simulates $LTCO_3$ spatially and seasonally in comparison to the ozonesondes and satellite instruments (i.e. typically within the ozonesonde variability and satellite uncertainty range).

References:

European Commission, Joint Research Centre, Dentener F, et al. 2016. Hemispheric Transport of Air Pollution (HTAP): specification of the HTAP2 experiments: ensuring harmonized modelling, Publications Office, https://data.europa.eu/doi/10.2788/725244.

Gaudel, A., Cooper, O. R., Ancellet, G., Barret, B., Boynard, A., Burrows, J. P., Clerbaux, C., Coheur, P. F., Cuesta, J., Cuevas, E., Doniki, S., Dufour, G., Ebojie, F., Foret, G., Garia, O., GranadosMunoz, M. J., Hannigan, J. W., Hase, F., Hassler, B., Huang, G., Hurtmans, D., Jaffe, D., Jones, N., Kalabokas, P., Kerridge, B., Kulwaik, S., Latter, B., Leblanc, T., Le Flochmoen, E., Lin, W., Liu, J., Liu, X., Mahieu, E., McClure-Begley, A., Neu, J. L., Osman, M., Palm, M., Petetin, H., Petropavlovskikh, I., Querel, R., Rahpoe, N., Rozanov, A., Schultz, M. G., Schwab, J., Siddans, R., Smale, D., Steinbacher, M., Tanimoto, H., Tarasick, D. W., Thouret, V., Thompson, A. M., Trickl, T., Weatherhead, E., Wespes, C., Worden, H. M., Vigouroux, C., Xu, X., Zeng, G., and Ziemke, J.: Tropospheric Ozone Assessment Report: Present day distribution and trends of tropospheric ozone relevant to climate and global atmospheric chemistry model evaluation, Elementa, 6, 1–58, https://doi.org/10.1525/elementa.291, 2018.

Hubert, D., Lambert, J-C., Verhoelst, T., Granville, J., Keppens, A., Baray, J-L., Bourassa, A.E., Cortesi, U., Degenstein, D.A., Froidevaux, L., Godin-Beekmann, S., Hoppel, K.W., Johnson, B.L., Kyrola, E., Leblanc, T., Lichtenberg, G., Marchand, M., McElroy, C.T., Murtagh, D., Nakane, H., Portafaix, T., Querel, R., Russell, J.M., Salvador, J., Smit, H.G.J., Stebel, K., Steinbrecht, W., Strawbridge, K.B., Stubi, R., Swart, D.P.J., Taha, G., Tarasick, D.W., Thompson, A.M., Urban, J., van Gijsel, J.A.E., Van Malderen, R., von der Gathen P., Walker, K.A., Wolfram, E. and Zawodny, J.M.: Ground-based assessment of the bias and long-term stability of 14 limb and occultation ozone profile data records. *Atmospheric Measurement Techniques*, 9, 2497-2534, doi: 10.5194/amt-9-2497-2016, 2016.

Keppens, A., Lambert, J-C., Graville, J., Hubert, D., Verhoelst, T., Compernolle, S., Latter, B., Kerridge, B., Siddans, R., Boynard, A., Hadji-Lazaro, J., Clerbaux, C., Wespes, C., Hurtmans, D.R., Coheur, P-F., van Peet, J.C.A., van der A, R.J., Garane, K., Koukouli, M.E., Balis, D.S., Delcloo, A., Kivi, R., Stubi, R., Godin-Beekmann, S., Van Roozendael, M. and Zehner, C.: Quality assessment of the Ozone_cci Climate Research Data Package (release 2017) – Part 2: Ground-based validation of nadir ozone profile data products. *Atmospheric Measurement Techniques*, 11, 3769-3800, doi: 10.5194/amt-11-3769-2018, 2018.

Figures and Tables:

Satellite	Quantity	Trend	Trend Lower	Trend Upper	p-value	Fit (R^2)
OMI – North America	Trend	-1.82	-16.33	12.66	0.80	0.58
	Trend Error 1	-3.47	-16.26	9.33	0.59	0.68
	Trend Error 2	-0.21	-16.12	15.73	0.98	0.50
	Apriori Trend	-0.12	-0.49	0.25	0.56	1.00
	UKESM Trend	0.49	-0.85	1.80	0.47	0.95
	UKESM+AKs Trend	-1.32	-3.65	1.04	0.26	0.90
	UKESM Trend Forced	1.69	0.51	2.89	0.00	0.95
	UKESM+AKs Trend Forced	-1.71	-4.37	0.92	0.20	0.89
FORLI – North America	Trend	-3.28	-5.43	-1.16	0.00	0.93
	Trend Error 1	-3.10	-5.11	-1.09	0.00	0.93
	Trend Error 2	-3.47	-5.80	-1.16	0.00	0.93
	Apriori Trend	0.00	-0.25	0.28	0.94	0.67
	UKESM Trend	-0.30	-1.73	1.13	0.67	0.93
	UKESM+AKs Trend	-0.74	-1.92	0.46	0.22	0.92
	UKESM Trend Forced	1.48	-8.09	11.02	0.76	0.46
	UKESM+AKs Trend Forced	1.27	0.18	2.38	0.02	0.93
SOFRID – North America	Trend	0.28	-1.36	1.89	0.74	0.94
	Trend Error 1	0.32	-1.36	2.03	0.70	0.90
	Trend Error 2	0.21	-1.11	1.52	0.75	0.94
	Apriori Trend	0.25	-0.39	0.90	0.43	0.98
	UKESM Trend	-0.55	-1.96	0.85	0.44	0.95
	UKESM+AKs Trend	-0.09	-1.22	1.04	0.87	0.97
	UKESM Trend Forced	1.85	0.95	2.75	0.00	0.97
	UKESM+AKs Trend Forced	1.34	0.55	2.13	0.00	0.98
OMI -Europe	Trend	-1.85	-16.84	13.14	0.80	0.71
	Trend Error 1	-3.81	-15.99	8.36	0.53	0.76
	Trend Error 2	0.12	-17.19	17.39	0.99	0.67
	Apriori Trend	-0.28	-0.60	0.07	0.10	1.00
	UKESM Trend	-0.25	-1.16	0.67	0.59	0.99
	UKESM+AKs Trend	-1.66	-4.09	0.74	0.16	0.95
	UKESM Trend Forced	1.43	0.32	2.54	0.01	0.98
	UKESM+AKs Trend Forced	1.09	-1.18	3.33	0.34	0.94
FORLI - Europe	Trend	-4.23	-6.42	-2.06	0.00	0.92
	Trend Error 1	-4.16	-6.28	-2.03	0.00	0.93
	Trend Error 2	-4.32	-6.63	-2.01	0.00	0.92
	Apriori Trend	0.21	-0.21	0.62	0.32	0.48

	UKESM Trend	-0.65	-1.78	0.46	0.25	0.98
	UKESM+AKs Trend	-0.99	-2.80	0.81	0.27	0.94
	UKESM Trend Forced	0.85	-0.12	1.82	0.08	0.98
	UKESM+AKs Trend Forced	0.65	-0.88	2.17	0.40	0.93
SOFRID - Europe	**Trend**	0.12	-2.10	2.33	0.92	0.93
	Trend Error 1	0.37	-1.71	2.47	0.72	0.91
	Trend Error 2	-0.16	-2.10	1.80	0.87	0.93
	Apriori Trend	0.39	-0.28	1.04	0.24	0.98
	UKESM Trend	-0.62	-1.66	0.44	0.24	0.98
	UKESM+AKs Trend	0.18	-0.76	1.13	0.69	0.98
	UKESM Trend Forced	1.06	0.21	1.94	0.01	0.99
	UKESM+AKs Trend Forced	0.23	-0.74	1.18	0.64	0.98
OMI – East Asia	**Trend**	-0.21	-18.20	17.79	0.98	0.51
	Trend Error 1	-2.43	-15.27	10.44	0.70	0.66
	Trend Error 2	2.01	-19.03	23.05	0.85	0.38
	Apriori Trend	-0.58	-1.64	0.51	0.29	0.98
	UKESM Trend	-0.37	-2.17	1.43	0.67	0.98
	UKESM+AKs Trend	-1.43	-5.17	2.31	0.44	0.95
	UKESM Trend Forced	2.08	0.79	3.40	0.00	0.99
	UKESM+AKs Trend Forced	2.36	-0.09	4.83	0.05	0.97
FORLI – East Asia	**Trend**	-3.51	-4.99	-2.03	0.00	0.93
	Trend Error 1	-3.28	-4.76	-1.80	0.00	0.93
	Trend Error 2	-3.74	-5.24	-2.26	0.00	0.92
	Apriori Trend	-0.07	-0.51	0.37	0.76	0.21
	UKESM Trend	-0.07	-1.43	1.29	0.93	0.98
	UKESM+AKs Trend	-0.67	-1.85	0.51	0.25	0.95
	UKESM Trend Forced	1.52	0.35	2.70	0.01	0.98
	UKESM+AKs Trend Forced	0.18	-1.02	1.41	0.75	0.93
SOFRID - East Asia	**Trend**	-0.44	-2.33	1.46	0.65	0.96
	Trend Error 1	-0.18	-1.69	1.34	0.82	0.90
	Trend Error 2	-0.69	-2.36	0.97	0.41	0.93
	Apriori Trend	-0.35	-0.90	0.21	0.21	0.98
	UKESM Trend	-0.97	-2.24	0.30	0.12	0.99
	UKESM+AKs Trend	-0.55	-1.55	0.46	0.28	0.98
	UKESM Trend Forced	1.46	0.60	2.31	0.00	0.99
	UKESM+AKs Trend Forced	0.46	-0.46	1.41	0.31	0.98

Table S1: *$LTCO_3$ trends (ppbv/decade) for the satellite trend (Trend), the satellite-uncertainty trend (Trend Error 1), the satellite+uncertainty trend (Trend Error 2), the satellite apriori trend (Apriori Trend), UKESM trend (UKESM Trend), UKESM with AKs applied trend (UKESM+AKs Trend), UKESM*

*forced trend (UKESM Trend Forced) and UKESM with AKs applied forced trend (UKESM+AKs Trend Forced). The "trend lower" and "trend upper" represent the trend 95% confidence interval based on the trend precision calculated from **Equation 3** in the main manuscript. R^2 is the trend fit skill (i.e. correlation squared) and the p-value is also shown.*

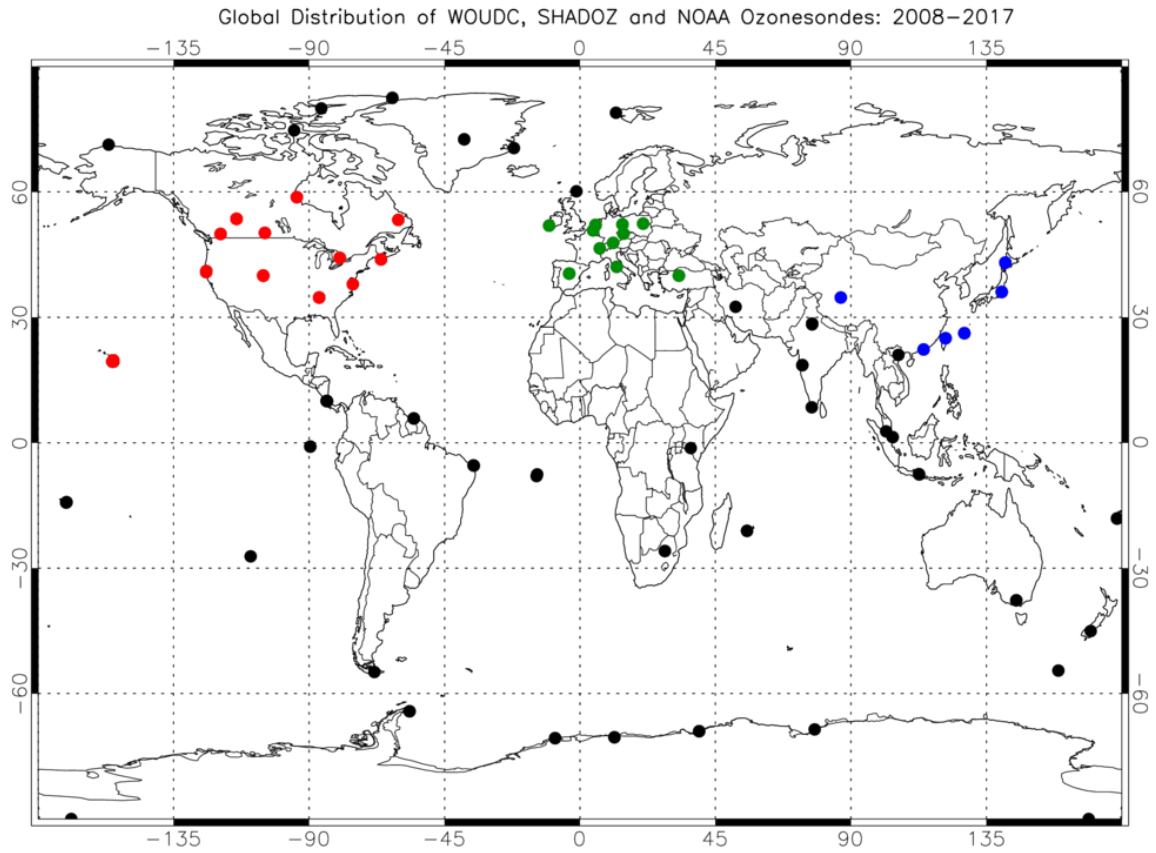

Figure S1: *Locations of the ozonesondes used for deriving the bias correction offsets (BCOs), evaluating UKESM and calculating regional lower tropospheric column ozone ($LTCO_3$) trends (Dobson units, DU). The red, green and blue ozonesonde sites were used for deriving the regional long-term time-series (2008-2017) for North America, Europe and East Asia, respectively (see **S2** for more details on region definitions). Note, several ozonesonde sites will have overlapping circles*.

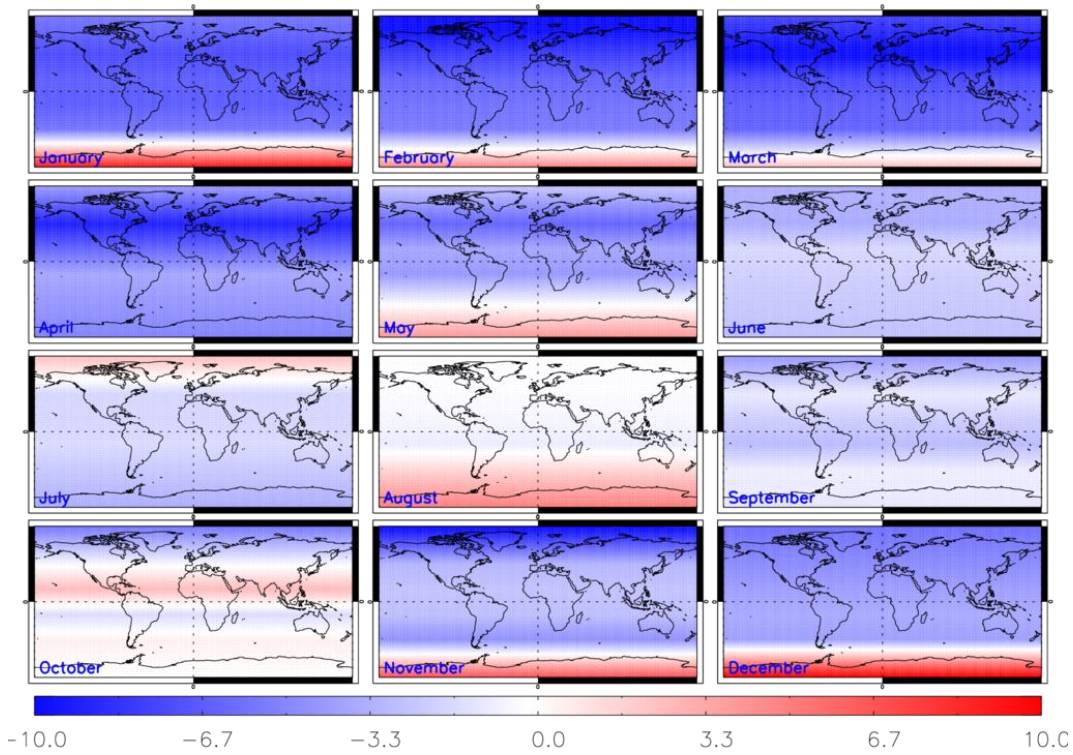

Figure S2*: OMI-ozonesonde (with AKs applied) bias correction offsets (BCOs, Dobson Units (DU)) for OMI lower tropospheric column O_3 ($LTCO_3$) using the instrument record between 2008 and 2017.*

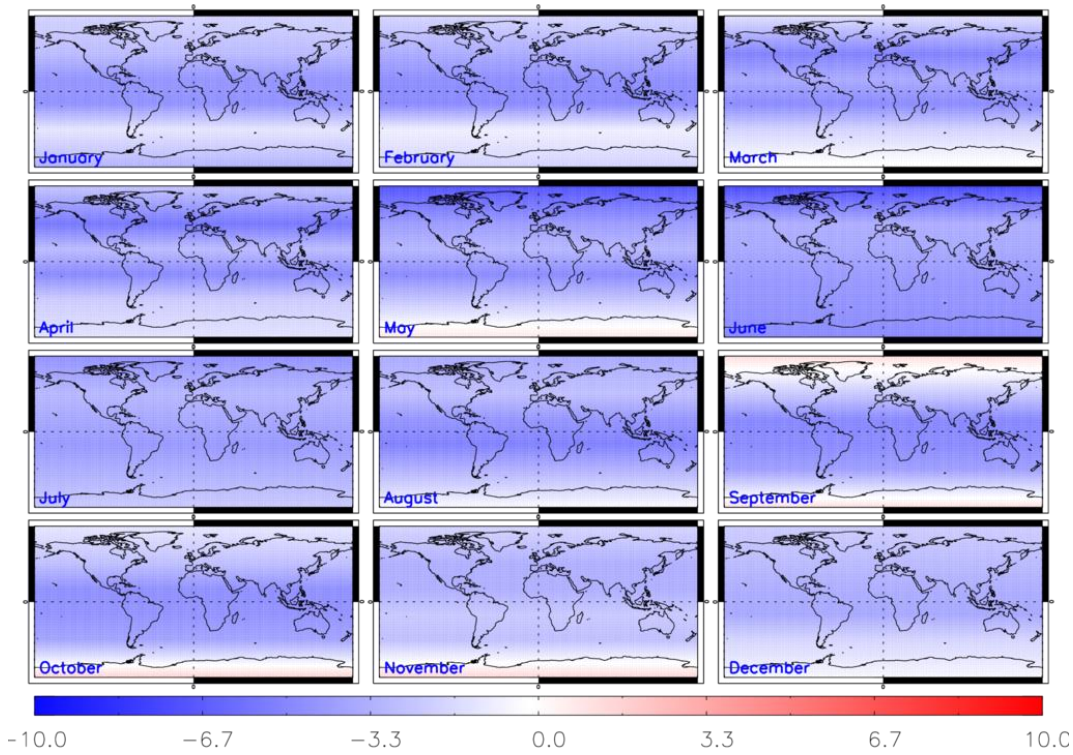

Figure S3*: IASI-FORLI - ozonesonde (with AKs applied) BCOs (DU) for IASI-FORLI LTCO₃ using the instrument record between 2008 and 2017.*

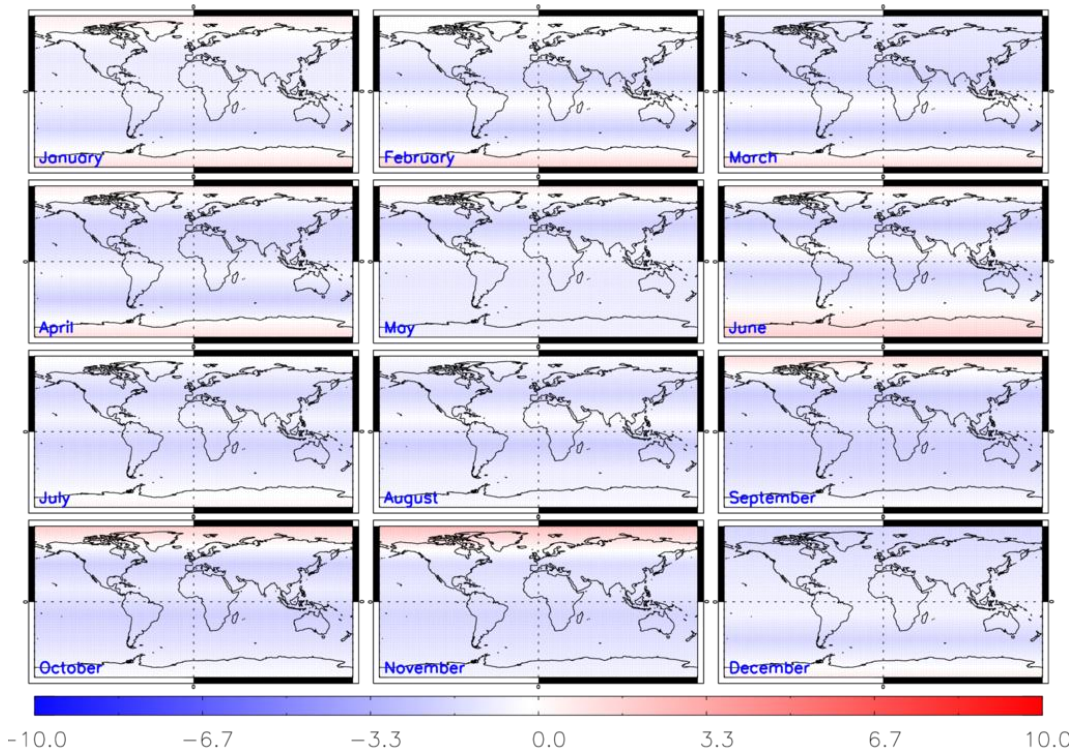

Figure S4: *IASI-SOFRID - ozonesonde (with AKs applied) BCOs (DU) for IASI-SOFRID LTCO$_3$ using the instrument record between 2008 and 2017.*

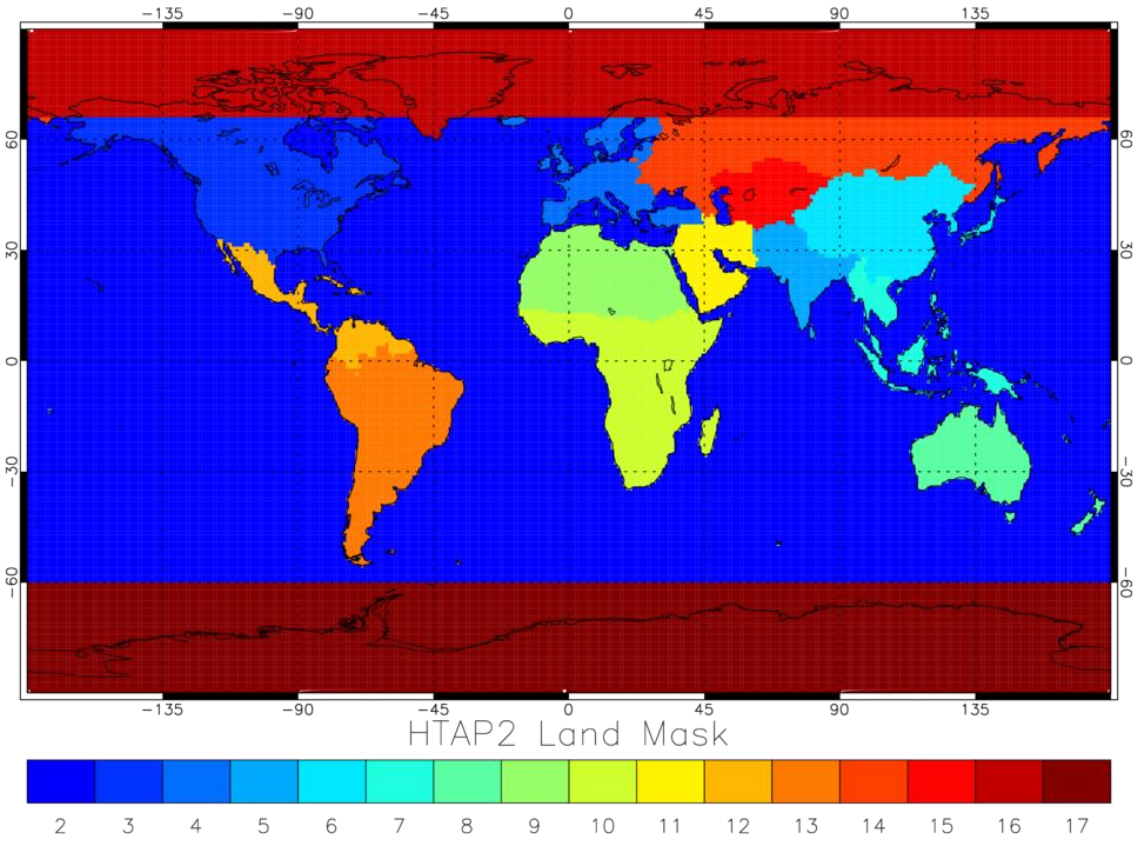

Figure S5: *Mask of different regions provided by the Task Force on Hemispheric Transport of* Air *Pollution (HTAP) on a 1°×1° horizontal resolution. For instance, mask code 4 represents Europe.*

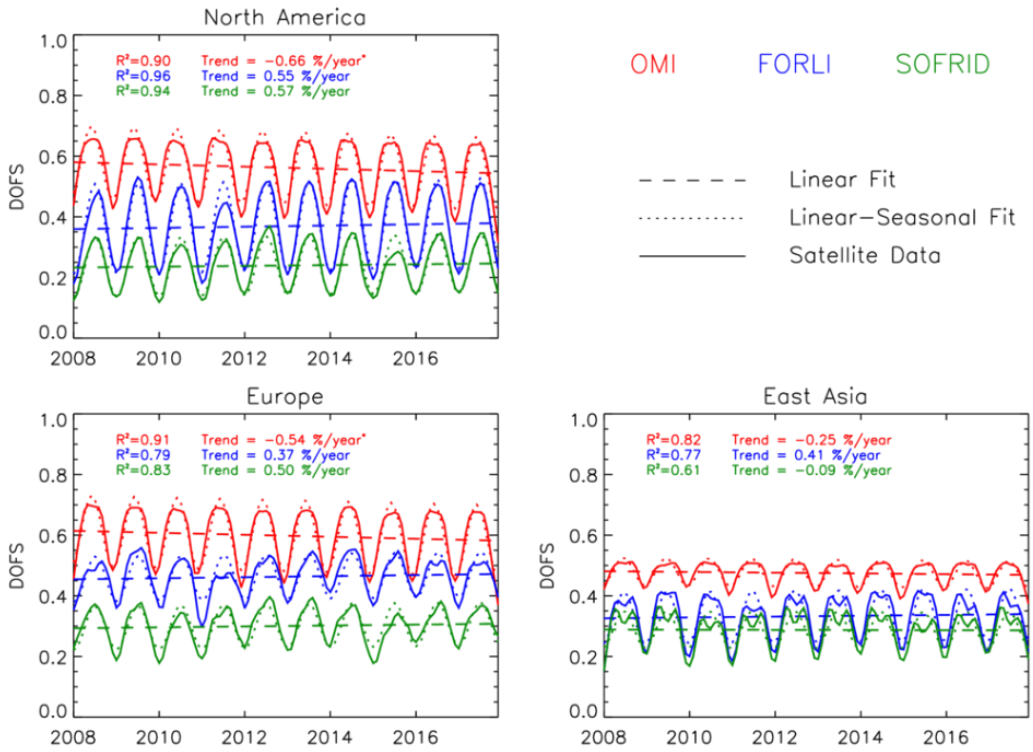

Figure S6: *Satellite degrees of freedom of signal (DOFS) for the surface to 450 hPa layer regional time-series for North America (top-left), Europe (bottom-left) and East Asia (bottom-right). OMI, IASI-FORLI and IASI-SOFRID DOFS time-series are shown in red, blue and green, respectively. Dashed lines show the DOFS linear trend which are labelled in the top of each panel. The R^2 squared values show the linear-seasonal trend model fit to the corresponding DOFS time-series (i.e. correlation squared). The * indicates where trends have a p-value < 0.05.*

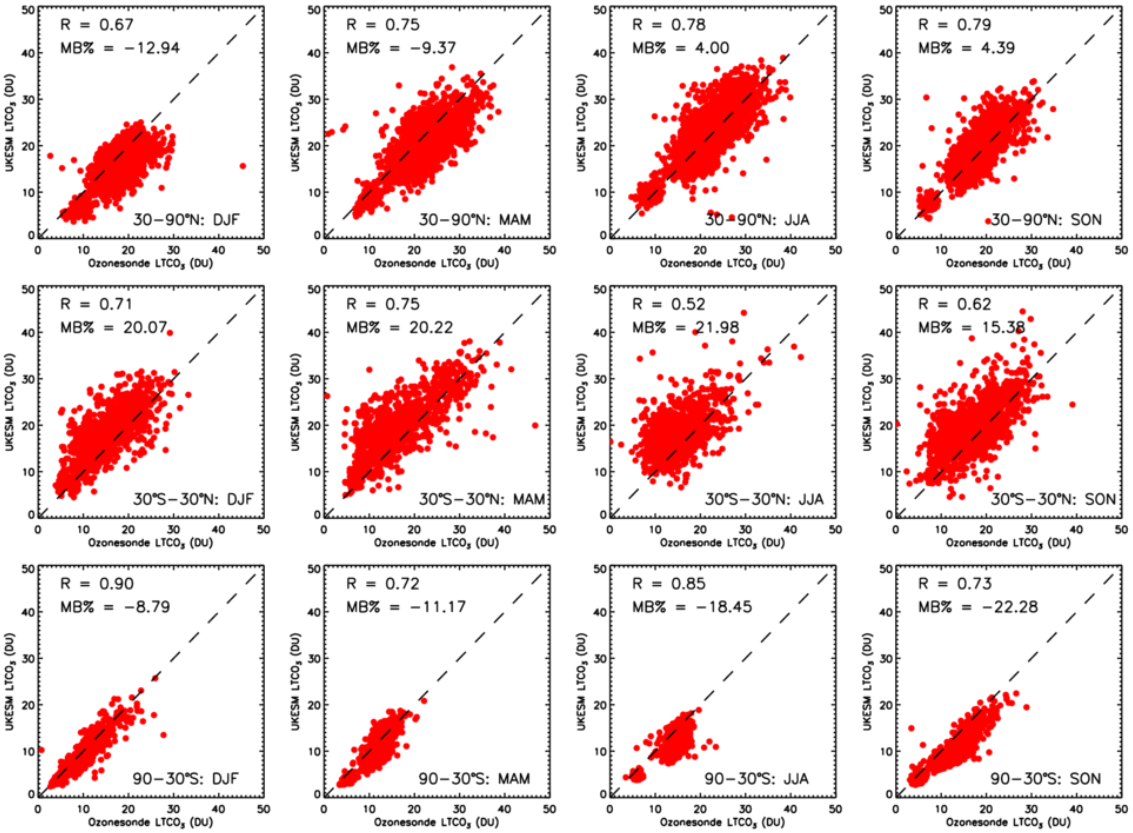

Figure S7*: Comparison of UKESM and ozonesonde $LTCO_3$ (DU) between 2008 and 2017 for December-January-February (DJF), March-April-May (MAM), June-July-August (JJA) and September-October-November (SON) across the latitude bands: 90-30°S, 30°S-30°N and 30-90°N. The correlation R and percentage mean bias (MB%) metrics are shown for each panel.*

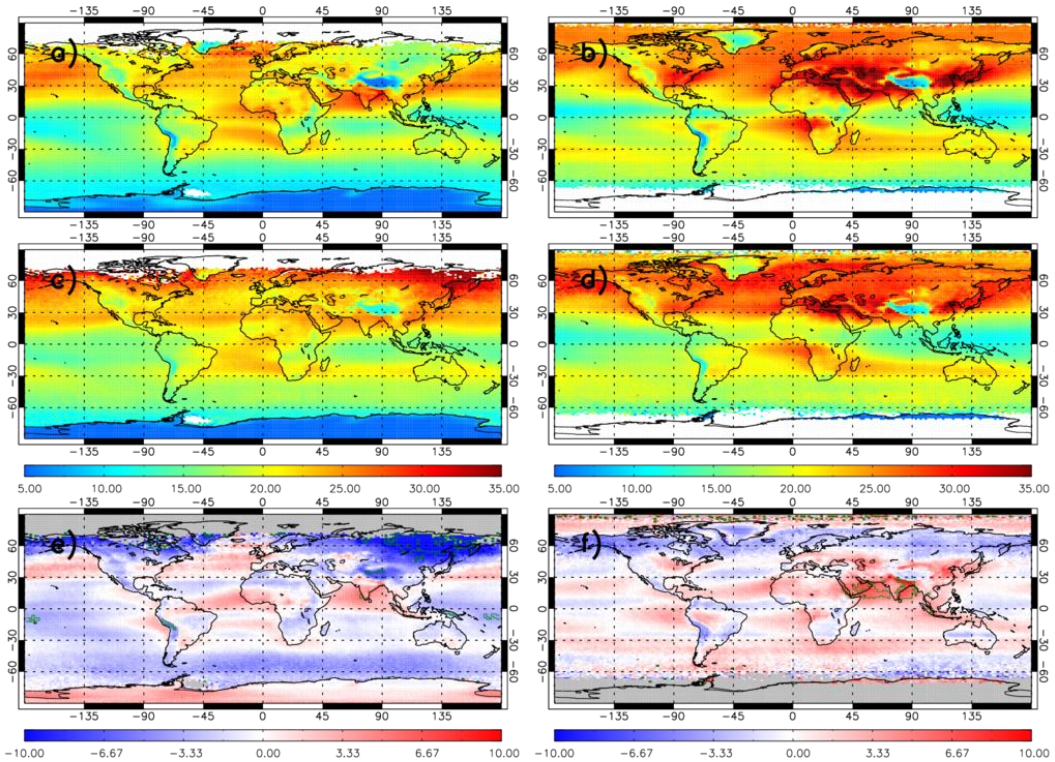

Figure S8: *$LTCO_3$ (DU) between 2008 and 2017 for a) UKESM with OMI averaging kernels (AKs) applied in DJF, b) UKESM with OMI AKs applied in JJA, c) OMI in DJF and d) OMI in JJA. Panels e) and f) show the UKESM-OMI mean bias for DJF and JJA, respectively. Green polygon-outlined regions show where the model-satellite biases are larger than the satellite error, but where the absolute bias is greater than 1.0 DU (i.e. focus on more substantial absolute biases).*

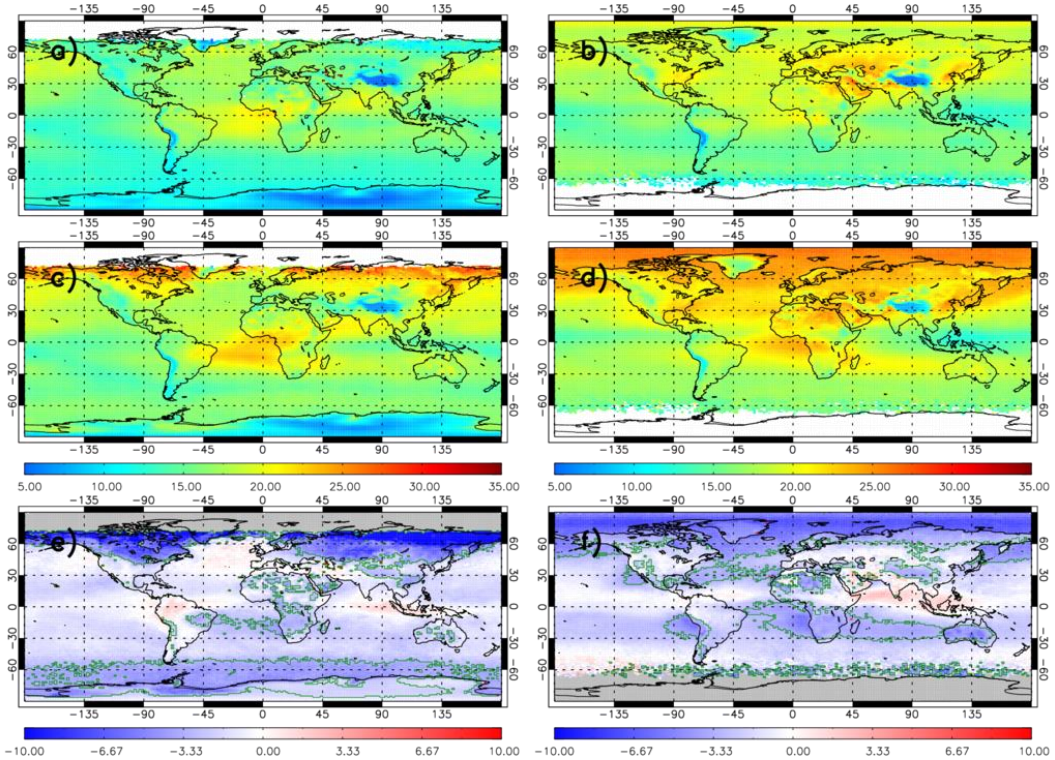

Figure S9: *Same as **Figure S8** but for IASI-FORLI $LTCO_3$ (DU).*

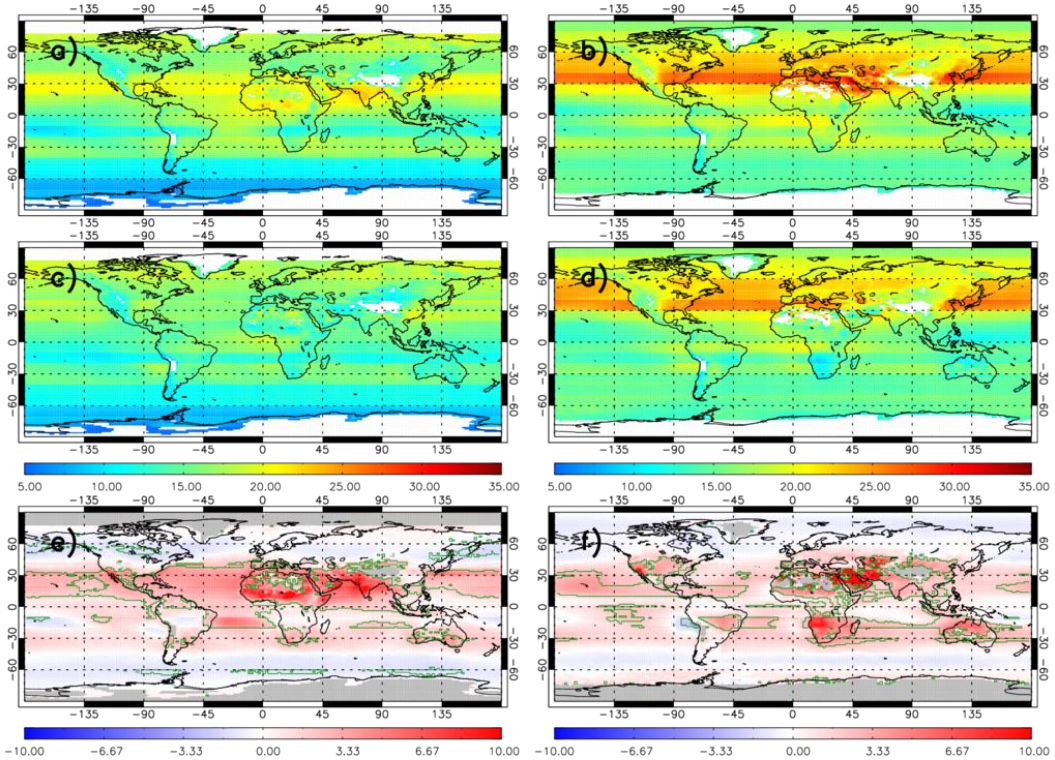

Figure S10: *Same as **Figure S8** but for IASI-SOFRID $LTCO_3$ (DU).*